Numerical Investigation of Automotive Paint Oven for Improving the Thermal Efficiency

Conference Paper · August 2022

DOI: 10.1115/FEDSM2022-88044

3 authors:

Mohammad-Reza Pendar
Universidade da Beira Interior
34 PUBLICATIONS **649** CITATIONS
SEE PROFILE

José Páscoa
Universidade da Beira Interior
256 PUBLICATIONS **2,447** CITATIONS
SEE PROFILE

Rui Lima
ccenergia
5 PUBLICATIONS **8** CITATIONS
SEE PROFILE

Proceedings of the ASME 2022
Fluids Engineering Division Summer Meeting
FEDSM2022
August 3-5, 2022, Toronto, Canada

FEDSM2022-88044

NUMERICAL INVESTIGATION OF AUTOMOTIVE PAINT OVEN FOR IMPROVING THE THERMAL EFFICIENCY

Mohammad-Reza Pendar
Center for Mechanical and Aerospace Science and Technology
University of Beira Interior
Covilhã, Portugal

José Carlos Páscoa
Center for Mechanical and Aerospace Science and Technology
University of Beira Interior
Covilhã, Portugal

Rui Lima
CCEnergia Lda
Rio Maior, Portugal

ABSTRACT

This study conducts a comprehensive numerical evaluation of conjugate heat transfer in an automotive paint oven to optimize the performance and increase the overall energy efficiency. Computational fluid dynamic (CFD) analysis of parameters in an automotive paint oven and on the coated vehicle surface is essential to achieve better paint quality and manufacturability, although the complicated geometry of vehicles, transient nature of the procedure, varying scales of the flow, and the tightly coupled conjugate heat transfer make the modeling difficult. An efficient computational algorithm, under the framework of the OpenFOAM package, using the Large Eddy Simulation (LES) turbulence model is implemented to numerically model the unsteady heated airflow behavior in the paint curing process. The conjugate heat transfer solver, chtMultiRegionFoam, is validated by heat sink case examination as heat transfer benchmark and then employed for the oven modeling. According to simulation results, the applied low-cost optimization of the intake hot flow rate and small oven geometry variation achieved significant energy efficiency improvement. During the optimization, the fluid dynamic characteristics, e.g., the mean temperature, velocity and streamline patterns, across all six zones of the oven, as well as the temperature and velocity map on a Body in White (BiW), are examined. The optimized arrangement and position of nozzles and panels for transient heat transfer processing of curing along the oven is described. Increasing the heated air provided by the panels on the lower half of the oven improves airflow circulation, resulting in a significant increment in the computed car body temperature.

Keywords: Automotive paint oven; Thermal efficiency; Conjugate heat transfer; Large-eddy simulation (LES); Paint curing

NOMENCLATURE

α_{eff}	Effective thermal diffusivity
h_s	Enthalpy solid
ρ_s	Solid density
ρ	Fluid density
$\tilde{u}_i$	Velocity vector
μ	Dynamic viscosity
t	time
h	Internal enthalpy
K	Kinematic energy
$\dot{R}_{heat}$	Heat generation
k_f	Fluid thermal conductivity
k_s	Solid thermal conductivity
T_f	Fluid temperature
T_s	Solid temperature
n	Normal direction to boundary
T_{hot}	Central fin base temperature
$\overline{Nu}$	Average Nusselt number
q''	Heat transfer flux
l	Fin characteristics length

1. INTRODUCTION

Paint curing, as one of the most critical steps in the automotive painting, refers to the drying procedure of the wet or powdered paint to a hard film. Solvent loss, oxidation, chemical reaction, melting and resolidifying are the most important ways of the paint film curing methods [1]. The temperature distribution, curing time and heat transfer rate are the main parameters in the curing process to prevent under curing or over curing and energy consumption optimization, considered in the paint cure window (PCW) [1, 2]. The final paint film quality is extremely related on the conveyor speed and the temperature distribution uniformity, which controlled by using empirical methods [3]. Automobile mass production involves the use of faster curing protectors. The ovens duty with optimal length is to supply the required heat for curing paint [4].

The most common causes of supplied heat losses include wall loss, waste gas loss, radiation loss at the entrance, and stored heat [5], which can be managed to reach minimum values. To guarantee development in oven efficiency, a deep numerical investigation of thermo-fluid-solid coupling turbulence treatment is needed. The simulation of the paint curing process in a continuous oven presents lots of complexities because of complex vehicle geometry, physical phenomena and flow scales. Rao and Teeparthi [6] introduced a dual solver, semi-computational method to predict the vehicle body temperatures in a paint drying oven. They considered the arrangement of the nozzles in the heat-up zone numerically to obtain a temperature map over the full BiW. Wu et al. [7] used an approximate transient approach of the intermediate steady solution to investigate a thermal transient of the car body curing. Also, their result has good agreement with the available experimental testing data. Mulemane et al. [8] propose reduced order models with lump capacities for the oven thermal modeling by manipulating related differential equations. Despotovic and Babic [9] present a simple mathematical model for automotive paint oven performance. Their model has the ability to examine the impact of various variables, which could help redesign the oven. Nazif [10] modeled the heat-up zone of the automotive wax oven and compared the result with their experimental measurement data. After some optimization, they increased 25% the energy efficiency of the considered oven. Xiao et al. [11] developed a novel cure window based proactive QC model for automotive topcoat curing. In their approach, film curing quality was assessed employing dynamic process-product models. Giampieri et al. [12] conducted a detailed examination of thermal management and energy efficiency to improve the energy consumption in the paint shop during automotive manufacturing.

The turbulent flow inside the curing oven, due to different velocity inlets range from nozzles and panels in different directions, selecting an appropriate turbulence model is very important [13,14]. The LES turbulence model is more suitable for capturing the principle of the internal flow and vortical structures [15, 16].

Figure 1 depicts the total energy consumption plant of conventional automotive manufacturing, divided into the paint shop, press shop chassis, powertrain, transmission and engine assembly, body shop and final assembly [17, 18]. The painting and ovening sections consume the most considerable energy during vehicle manufacturing processes. The paint shop gives BIW a pleasant finish and protection against weather and corrosion and because of that is so important.

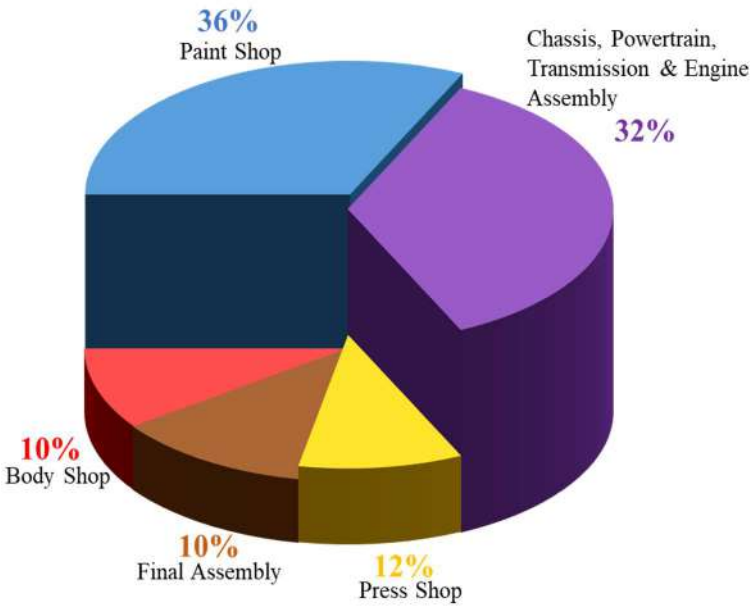

FIGURE 1: SCHEMATICS VIEWS OF A CONVENTIONAL AUTOMOTIVE MANUFACTURING WITH A BREAKDOWN OF THE TOTAL ENERGY CONSUMPTION.

2. GOVERNING EQUATIONS

The governing equations implemented in the present work can be divided into two phases: solid region (BiW & conveyor, nozzle's base wall) and fluid region (air inside the oven and injected hot air circuits). Then, coupling of the energy equations in the solid and fluid phases region are evaluated.

2.1 SOLID REGION

The gradient of temperature in the solid region can be achieved by using an energy balance in a suitable differential control volume. The following is the heat conduction equation that is solved for the solid region:

$$\frac{\partial}{\partial t}(\rho_s h) = \nabla \alpha_{eff} \nabla h, \quad (1)$$

where α_{eff}, h_s and ρ_s are the effective thermal diffusivity, enthalpy and density of the solid area, respectively.

2.2 FLUID REGION

The continuity, momentum and energy equations are solved within the fluid region. The Large Eddy Simulation (LES) turbulent model is used to handle the severe strain and stress rate of the complex flow inside the oven. An LES turbulence model is retained by applying "one equation eddy viscosity model" (OEEVM) subgrid-scale method [19, 20]. The following equation represents filtered continuity and momentum and energy equations, respectively, that employed in the LES turbulence model:

$$\frac{\partial \bar{\rho}}{\partial t} + \frac{\partial}{\partial x_j}(\bar{\rho}\tilde{u}_i) = 0, \quad (2)$$

$$\frac{\partial \bar{\rho}\tilde{u}_i}{\partial t} + \frac{\partial}{\partial x_i}(\bar{\rho}\tilde{u}_i\tilde{u}_j) = -\frac{\partial \bar{p}}{\partial x_i} + \frac{\partial}{\partial x_j}\tilde{\sigma}_{ij} - \frac{\partial}{\partial x_j}\rho(\widetilde{u_i u_j} - \tilde{u}_i\tilde{u}_j), \quad (3)$$

$$\tilde{\sigma}_{ij} = \bar{\mu}\left(\frac{\partial \tilde{u}_i}{\partial x_j} + \frac{\partial \tilde{u}_j}{\partial x_i} - \frac{2}{3}\delta_{ij}\frac{\partial \tilde{u}_k}{\partial x_k}\right), \quad (4)$$

$$\frac{\partial}{\partial t}(\bar{\rho}h) + \nabla(\bar{\rho}\tilde{u}_i h) + \frac{\partial}{\partial t}(\bar{\rho}K) + \nabla(\bar{\rho}\tilde{u}_i K) - \frac{\partial \bar{p}}{\partial t} = \nabla \alpha_{eff}\nabla h + \dot{R}_{heat}. \quad (5)$$

where ρ, $\tilde{u}_i$, μ and t are density, velocity vector, dynamic viscosity and time, respectively. Also, energy equation (Eq .5) is solved for internal enthalpy, h, in which K, $\dot{R}_{heat}$ and α_{eff} are kinematic energy, heat generation due to reactions and effective thermal diffusivity, respectively. More details about fluid region equation can be found in Pendar and Páscoa [21]. At the solid-fluid interface, since there is no surface reaction, the heat fluxes must fulfill the conservation of energy, i.e.,

$$k_f \frac{\partial T_f}{\partial n} = k_s \frac{\partial T_s}{\partial n} \quad (6)$$

where k and n are the thermal conductivity on each side and the direction normal to the boundary, respectively.

3. NUMERICAL IMPLEMENTATION SETUP

Figure 2 shows the schematic structure of the employed curing oven. As shown in this figure, the oven consists of three zones of heat-up, holding and cooling, which are designed to heat the body, maintain a steady temperature, and eventually cool down the treated body, respectively. The analogy between the current structure and an existing automotive oven is applied, and the inlets air flow rate and temperature distribution validate with data in real condition in various zones. The oven configuration had a total length of 53 meters; details of each zone are specified in Table 1. In heat-up, the temperature reaches the point of the paint solvent vaporization and provides paint curing at the molecular level. The oven heat a BiW by mostly convection modes. As shown schematically in Fig. 2, 3, 4 and data reported in Table 1(a), inside the oven is heated by hot air circuits, using heated walls, supply hot air nozzles and panels. In addition to the recirculating hot air circuits, fresh air and relatively cooler air are replenished from the two ends of an oven and circulated to compensate for the reduced air. The equivalent volume of air flow is evacuated from the return air ducts positioned at the top in a cross-wise direction to the axial direction zone. As shown in Fig. 1, the heated air continuously supplied by fan, passes through the tubes and sent to the air nozzles and panels to compensate for heat losses. In addition, the burned energy resources in three burners pass through heat exchanger tubes and exit to the atmosphere.

The parameters of the heat exchanger stream (air flow rate, velocity and temperature) for boundaries of the considered oven (six zones) before modification are summarized in Table 1(a). The hot re-circulating air was blown inside the oven through a set of nozzles and panels in zones 1 to 3, and panels in zone 4 and 5, are located on the walls. The hot air temperatures of the wall-mounted nozzles and panels in various zones ranged from 190 °C to 220 °C, and the turbulent flow velocities ranged from ≈ 3.0 m/s to 21 m/s. Also, the outlets are specified as pressure boundaries. In Table 1 (b), the quantity and size of all components of the investigated oven are detailed.

TABLE 1. PRELIMINARY OVEN OPERATING CONDITIONS IMPLEMENTED IN THE CURRENT SIMULATION.

(a)

		Inlet	**Zone 1**		**Zone 2**		**Zone 3**		**Zone 4**		**Zone 5**		**Zone 6**	
		Natural Air	Upper Hot Air	Lower Return Air	Hot Air	Return Air	Hot Air	Return Air	Hot Air	Retur n Air	Hot Air	Retur n Air	Cold Air	Return Air
Air Flow Rate	**$\dot{m}$(m^3/h)**	7900	5500	3000	65000	65000	23000	23000	46000	46000	100	100	25000	27560
Mean Air Velocity	**U_{mean} (m/s)**	0.341	20.57	11.20	3.107	8.377	3.477	5.926	3.353	6.238	0.2	0.2	11.54	9.4325
Mean Air Temperature	**T (°c)**	30	195	195	220	190	220	190	220	190	195	195	20	50
Zone Length	**L(m)**	-	1.2		18.5		10		17		1.4		5	

(b)

	Inlet	Zone 1		Zone 2			Zone 3			Zone 4		Zone 5		Zone 6	
	Natural Air Inlet	Upper Air Panel	Lower Air Panel	Air Nozzles	Air Panels	Return Air Ducts	Air Nozzles	Air Panels	Return Air Ducts	Air Panels	Return Air Ducts	Upper Air Panel	Lower Air Panel	Cold Air Fan	Return Air Ducts
Number (N)	1	1	1	60	108	20	30	32	12	88	18	2	2	144	12
Mean Area (A (m^2))	6.43	0.074	0.074	0.8347	4.976	2.155	0.4174	1.787	1.293	3.81	2.048	0.856	0.852	0.772	0.81

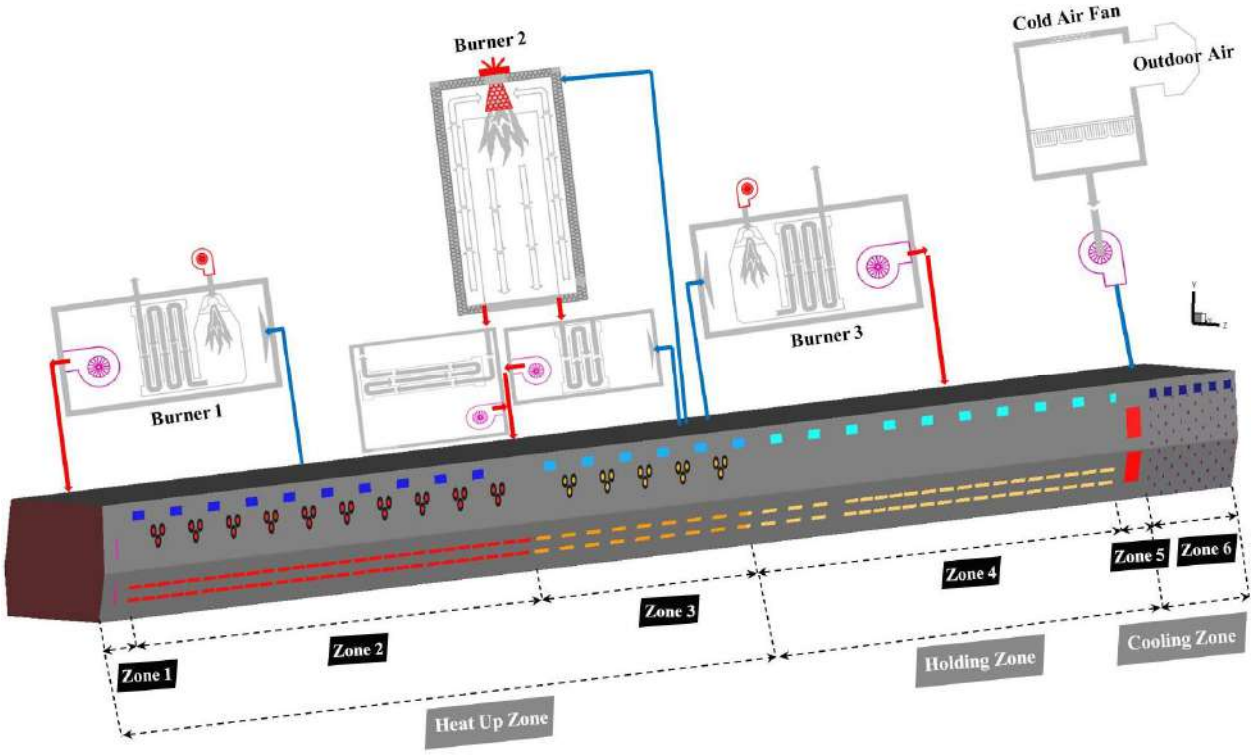

FIGURE 2: SCHEMATIC DRAWING OF OVEN GEOMETRY CONFIGURATION WITH ALL HEAT UP, HOLDING AND COOLING ZONES.

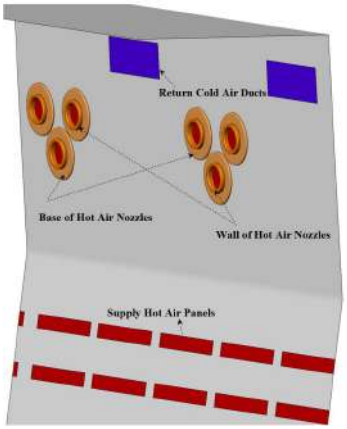

FIGURE 3: POSITION OF HOT AIR NOZZLES' S COMPONENTS: BASE AND WALL.

Figure 5 shows a comprehensive illustration of a computational grid for a full curing oven, including various close-up views. All areas of the computational domain inside the oven, despite many complexities, are generated with a fully structured quadrilateral mesh, exept in the cumputational region with presence of BiW. The domain is decomposed into fifty-four smaller sub-sections over the six zones. The near boundaries and wall mesh size significantly influence the Conjugate Heat Transfer (CHT) predictions. After mesh independence analysis for the mean temperature and velocity distribution, we concluded that a simulation using the grid with an overall account of ≈ 40 million cells is appropriate.

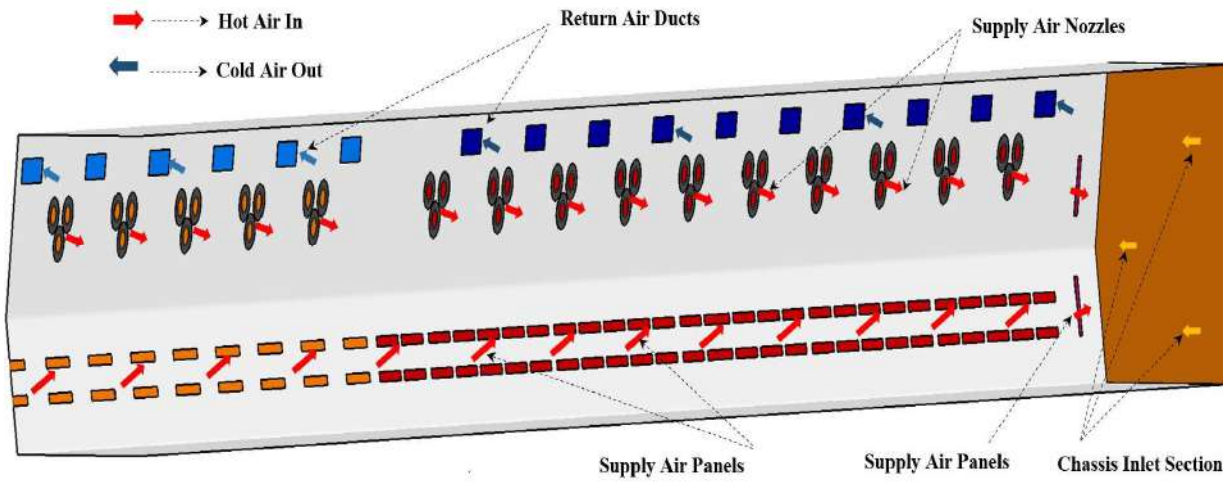

FIGURE 4: COMPUTATIONAL DOMAIN OF HEAT UP ZONES WITH ALL COMPONENTS OF SUPPLY AIR NOZZLES, SUPPLY AIR PANELS, RETURN AIR DUCT, AND CHASSIS INLET SECTION.

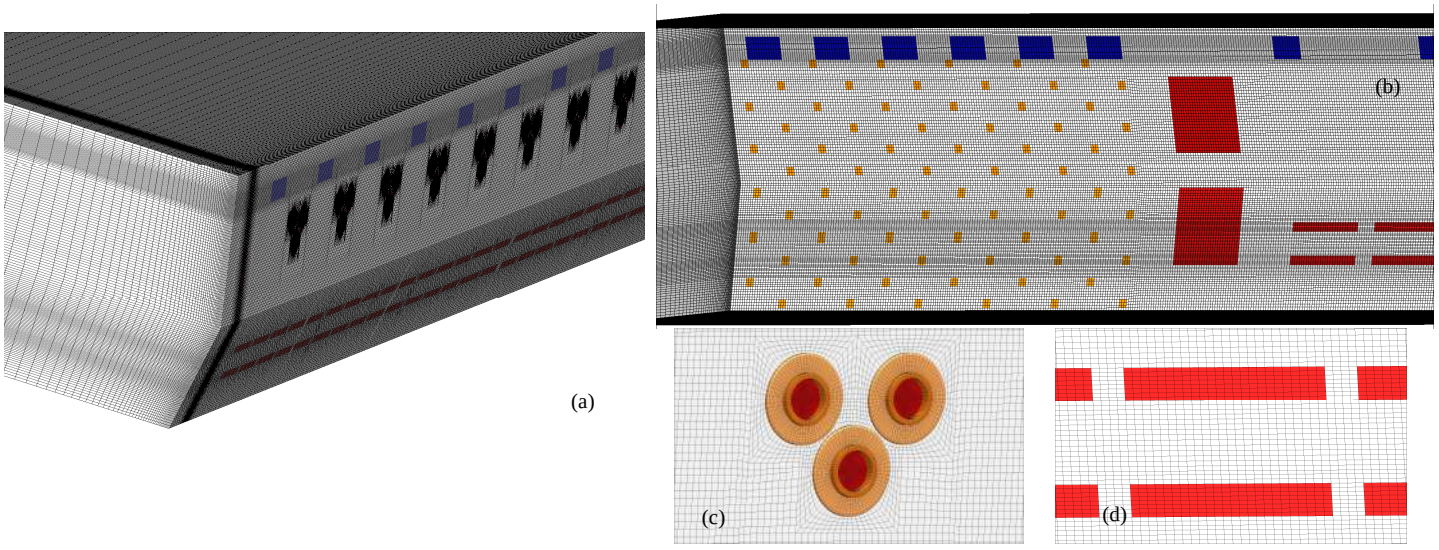

FIGURE 5: GENERATED VOLUME MESH DURING THE COMPUTATIONAL DOMAIN OF THE OVEN.

4. THE CHTMULTIREGIONFOAM VALIDATION

Before presenting the results of turbulent flows in the automotive curing oven, a transient 3D heat convection problem in the heat sink, including heat conduction in fins, is considered to validate the accuracy of the employed code. The boundary conditions and dimensions of the computational domain are illustrated in Fig. 6 (a), as considered in reference [22]. The size of the domain is 600 mm^3, and atmospheric pressure condition is applied to all-round surfaces. The length of the domain is around 43 times larger than the height of the heat sink. A constant temperature is applied to the base of the heat sink. The structure grid used in this case has approximately 8.6 million cells, as shown in Fig. 6 (b).

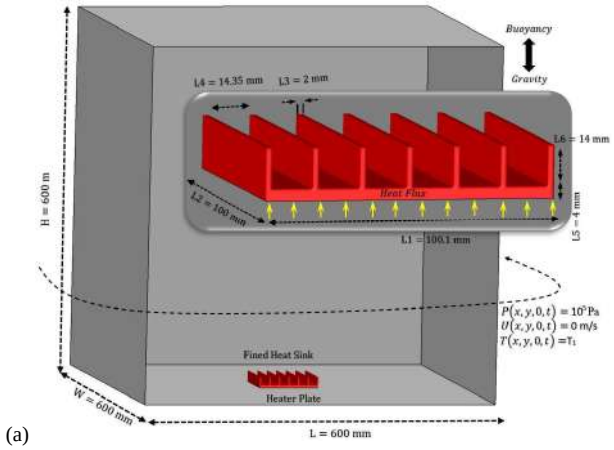

(a)

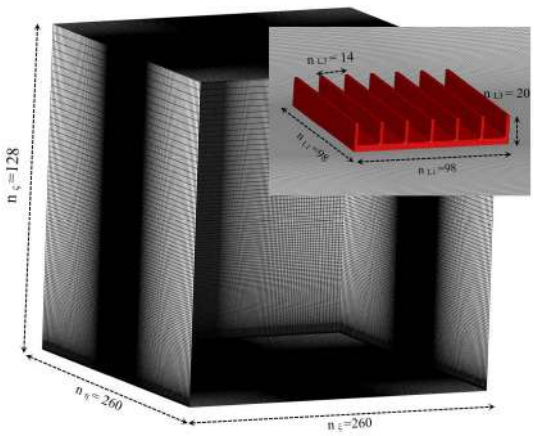

(b)

FIGURE 6: (a) DIMENSIONS AND BOUNDARY CONDITIONS OF THE HEAT SINK, AND (b) 3D VIEWS OF THE COMPUTATIONAL GRID, WITH CLOSE-UP VIEWS OVER THE FINS.

Table 1 depicts the conditions of five different heat power cases for the heat sink, including room temperature (T_∞) and central fin base temperature (T_{hot}). As a validation purpose, Fig. 7 compares current numerical results, experimental data of da Silva et al. [22] and analytical reports of Harahap and Rudianto [23] for the average Nusselt number and the average heat transfer coefficient. Average heat transfer ($\bar{h} = q''/(T_{hot} - T_\infty)$) and Nusselt number ($\overline{Nu} = \bar{h}.l/k$) are obtained through the NusseltCalc tool [24]. q'', k *and* l *are* the heat transfer flux between the heatsink and the fluid, the air thermal conductivity and $l = L_2/2$, respectively. The difference between the obtained numerical results and experimental in the majority of the cases is lower than 7 % and are close to the analytical values. As a result, a good agreement is obtained. This agreement verified the use of OpenFOAM as a reliable tool to study conjugate heat transfer (conduction and free convection) problems in the automotive curing oven.

TABLE 1. THE TEMPERATURE SETTINGS FOR THE CASES USED IN THIS SIMULATION.

Case	T_1 [k]	T_2 [k]	ΔT [K]
A	295.94	304.30	8.36
B	296.29	310.92	14.63
C	295.63	322.07	26.44
D	297.16	348.32	51.16
E	295.45	369.26	73.81

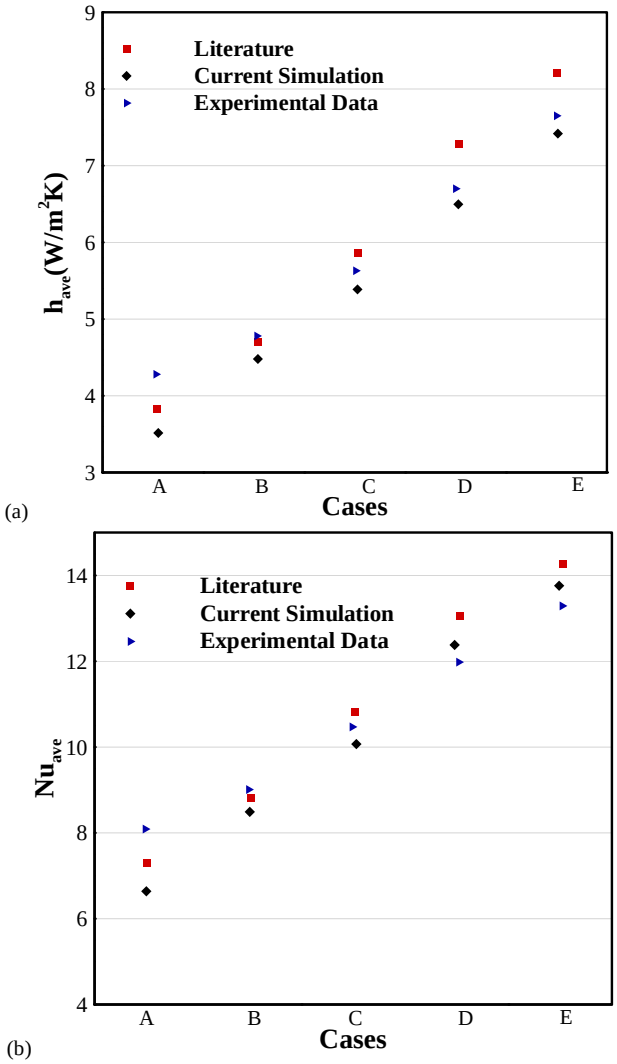

FIGURE 7: COMPARISON OF THE (A) AVERAGE NUSSELT NUMBER AND (B) AVERAGE HEAT TRANSFER COEFFICIENT (T=5 S): CURRENT NUMERICAL RESULTS, EXPERIMENTAL DATA (DA SILVA ET AL. [22]) AND LITERATURE REPORTS (HARAHAP AND RUDIANTO [23]).

The heat generated by the sink is conducted to the fins and exchanged with the surrounded fluid. The fluid temperature gradient increases due to the convection, as shown in Fig. 8.
The formation of a small recirculation area near the heat sink, after that, a large recirculation region involving the entire domain is visible in Figure 8 (a). The distance between the fins is sufficient to produce two counter-rotating vortices. In this case, due to the large space among fins, the convection flow decreases. Figure 8 (c) shows a 15% reduction in air density between fins compared to room density (1.17 kg/m3), making the air to ascend in this area.

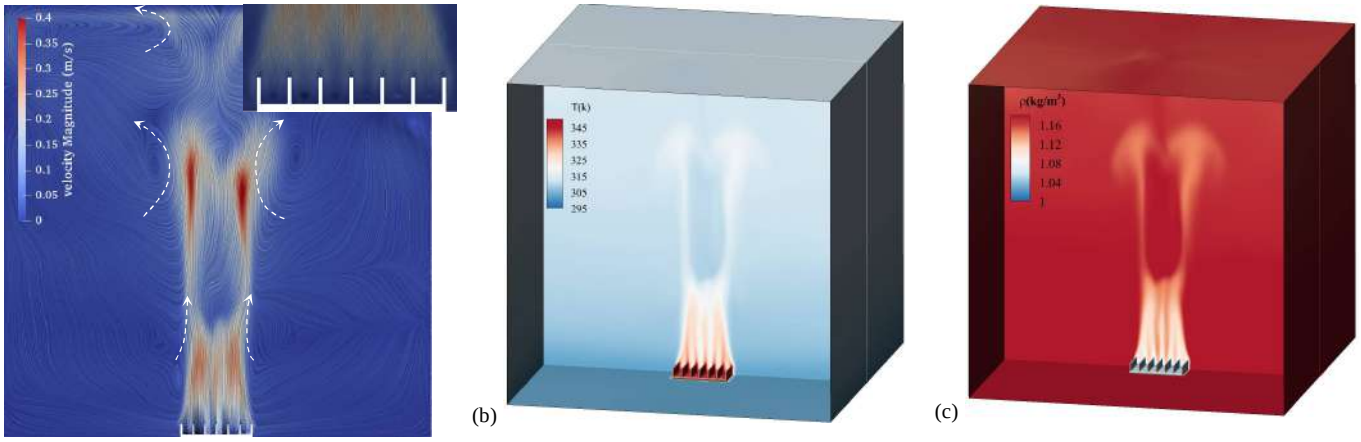

FIGURE 8: (a) VELOCITY FIELD WITH STREAMLINES (LIC METHOD VISUALIZATION [25]), (b) TEMPERATURE FIELD, AND (c) DENSITY FIELD OF CASE (D) AROUND HEAT SINK.

5. RESULTS AND DISCUSSION

The results describe the curing of the electrodeposition coating process on the BiW in an automotive oven. A real industrial automotive curing oven with a car body (Citroën Berlingo) is used. The mean hot air temperature contour on cross-section at the positions of nozzles, panels and return air duct with the presence of the BiW chassis is shown in Fig.9. The temperature contour on the BiW surface during the initial curing phase proves that the hood and rocker of the body require more care than the side body, which can be provided with the redirection of the panels and nozzles hot airflow. As the figure shows, the temperature distribution on the car body outer shell due to the complicated structure is highly non-uniform. The transmission transfer is higher around the nozzle and panel region, on the exterior of the BiW surfaces such as the doors and fender.

The mean air temperature contour in the cross section of the center plane along with the oven's length, is shown in Fig. 10. Proper feeding of hot air with adequate circulation and convection in zones 1&2 is apparent. Each zone has an almost uniform temperature range without any severe jump, including gradual longitudinal gradient. But, a weak supply of hot air in zone 3 of the heat-up region, particularly in the lower height half of the oven, due to the low density of the panel, leads to a poor air operation and lower average temperature increment.

Figure 11 illustrates the mean air temperature distribution on the center planes that are normal to the curing oven length. The qualitative behavior of the computed temperature curves is similar to what is expected from the curing oven. After surging temperature during the heat-up zones, the temperature remains almost constant at the holding area before plummeting in the cooling zone. However, these stages have some design and oscillation weaknesses, which are improved in the modified case (Fig.11 c-e). Improvement activities for hot air redirection for proper conduction and appropriate hot air flow rate adjustment are considered in our study. The investigated height values of 0.4 m, 1 m and 1.2 m are at the rocker, character line and the roof of the BiW. For describing the modified oven changes, 15 percent removal and addition of injected flow rate from upper components to lower components in zones 1, 2, 3 and 6, correspondingly, can be mentioned. In zones 1, 2 and 3 that have both hot air panels and nozzles, and zone 6, which has two series of upper and lower cold air fans, hot and cold airflow share manipulation is implemented. These modifications were made to allow for better convection, at the same amount of the hot airflow rate generation, which originated from the burners. As illustrated in Fig. 11 (c-e), this modification results in better hot thermal flow directed precisely to the BiW surface, without extra costs and with the same level of energy consumption.

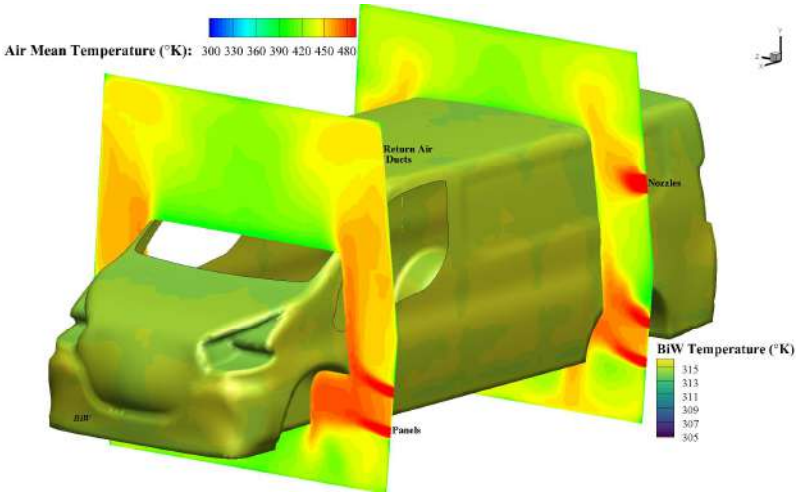

FIGURE 9: MEAN TEMPERATURE DISTRIBUTION ON THE BIW SURFACE ($L = 9.5\,m$) AND TWO 2D PLANES ($L_1 = 8.3m$, $L_2 = 11m$) AT THE HEAT-UP PHASE IN THE OVEN ($t = 1Min$).

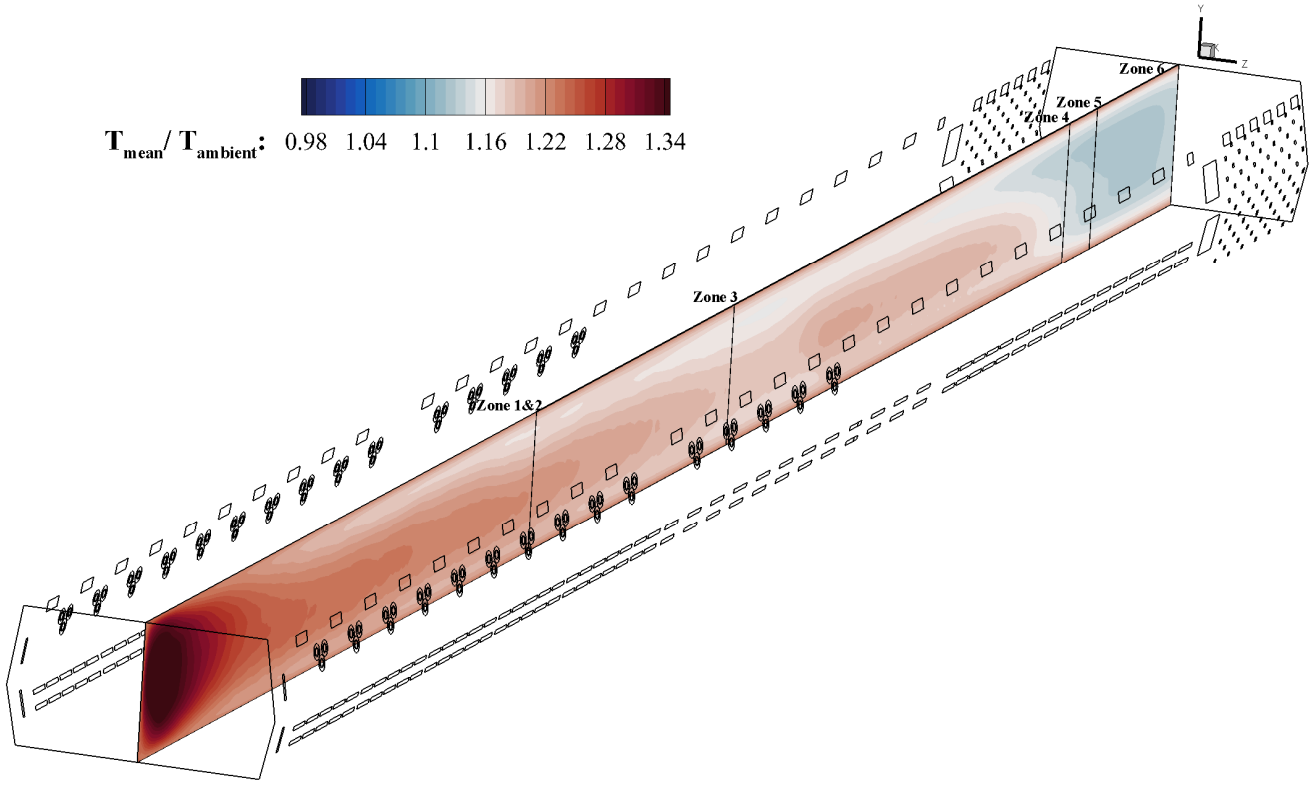

FIGURE 10: MEAN AIR TEMPERATURE (°K) CONTOURS, NORMALIZED BY THE AMBIENT AIR, ALONG THE Full LENGTH OF THE OVEN'S CENTER PLANE ($L = 52\,m$) AFTER $t = 3\,Min$.

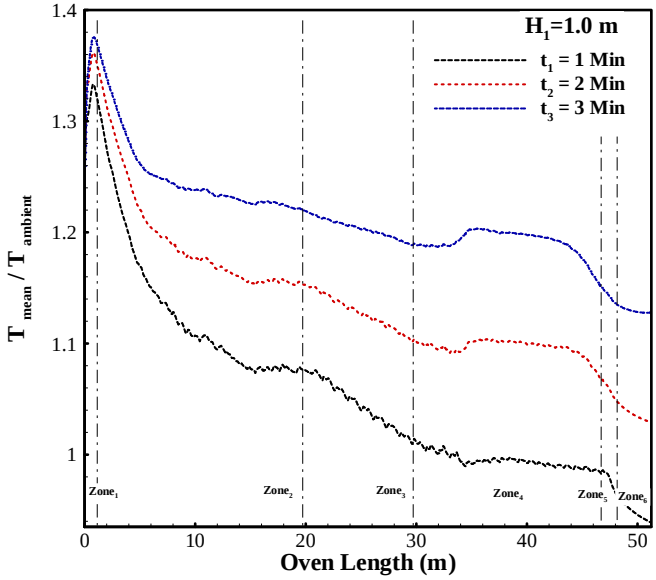

(a)

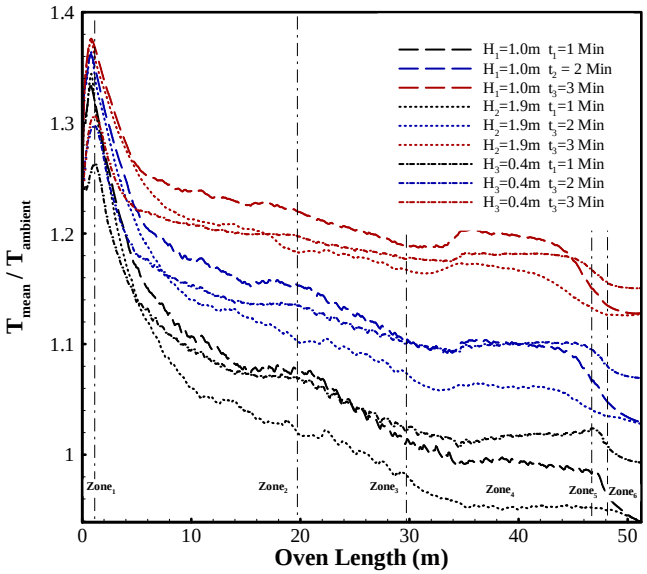

(b)

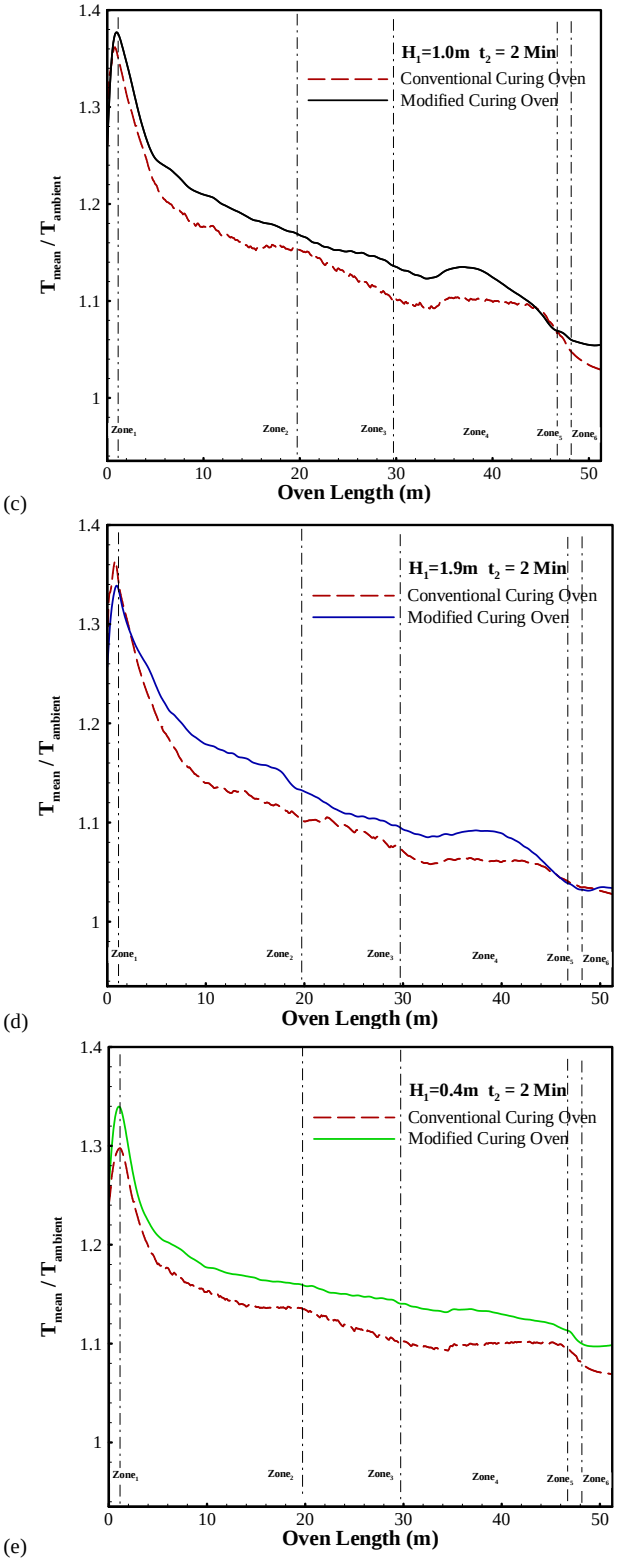

FIGURE 11: NORMALIZED MEAN TEMPERATURE (°K) DISTRIBUTION ALONG WITH THE CURING OVEN: (A) TEMPORAL EVOLUTION, (B) HEIGHT ASSESSMENT AND (C-F) MODIFIED OVEN COMPARISON.

As a positive point for the presented simulated oven, the heated air with low-speed interaction with the BiW in the heat up and holding zones, after the first high pressure hot air injection at the entrance (Zone 1). This condition provides an appropriate time for the oven to exchange heat by the BiW and allows to obtain paint film with higher finishing quality. The higher velocity in the cooling zone is apparent in comparison to other zones.

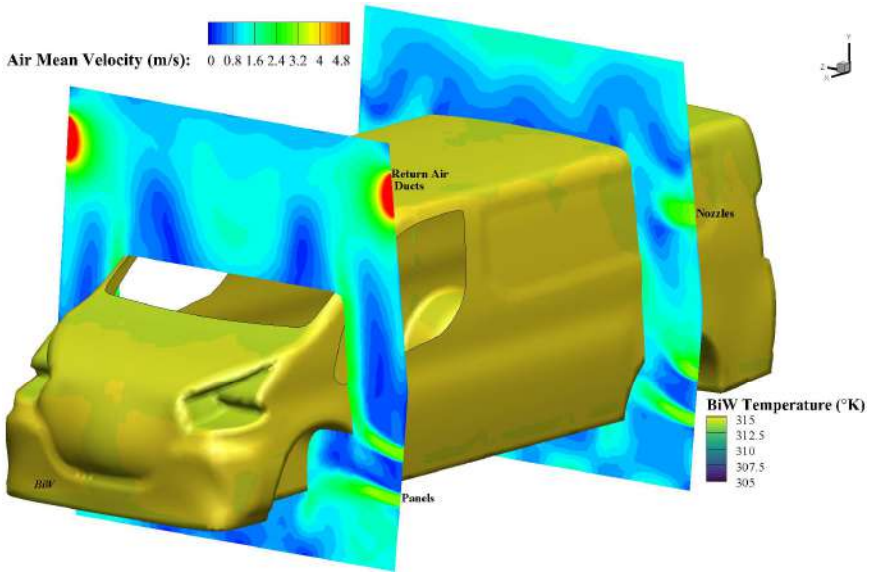

FIGURE 12: MEAN AIR VELOCITY CONTOURS IN A CROSS-SECTION AT TWO PLANES ($L_1 = 8.3m$, $L_2 = 11m$) AFTER $t = 1Min$.

The recognition of flow vortical structures and streamlines patterns during the accurate oven simulation with the precise LES turbulence model is helpful for engineering and qualitative evaluation. By considering the vortical structure patterns and streamlines path in Fig.15, visualized by the LIC method [25], the convection flow's intensity and power from the oven's lower to the upper side can be detected. This significantly help us to manage the flow and introduced modified cases. The existence of the large circulation vortexes (as illustrated in Fig. 15), originating from panels, nozzles and fans, have an adequate effect of quick BiW warm-up and chilling. The large size of the recirculation zones (Fig. 15) increases the injected hot air efficiency and contact on the BiW surface.

By mentioned modification (described in Fig.11), the optimized circulation turns sketched from the lower panel intensified and accident more cover of the BiW surface and more heat transfer chances (Fig. 12, 13). According to Fig. 14 and 15, the streamlines congestion at two ends of the curing oven, zone 1&2 and 6, provides more thermal manipulation on the BiW surface.

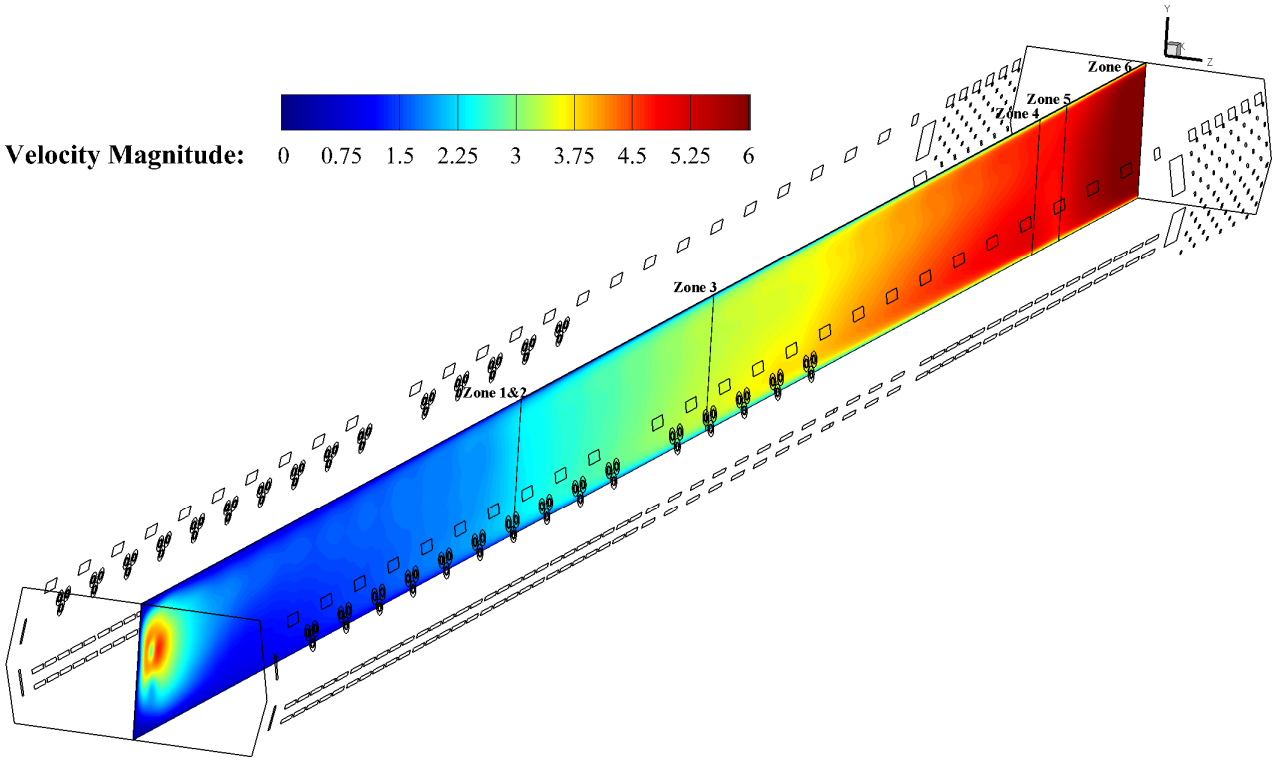

FIGURE 13: MEAN AIR VELOCITY (m/s) CONTOURS ALONG THE Full LENGTH OF THE OVEN'S CENTER PLANE ($L = 52\,m$) AFTER $t = 3\,Min$.

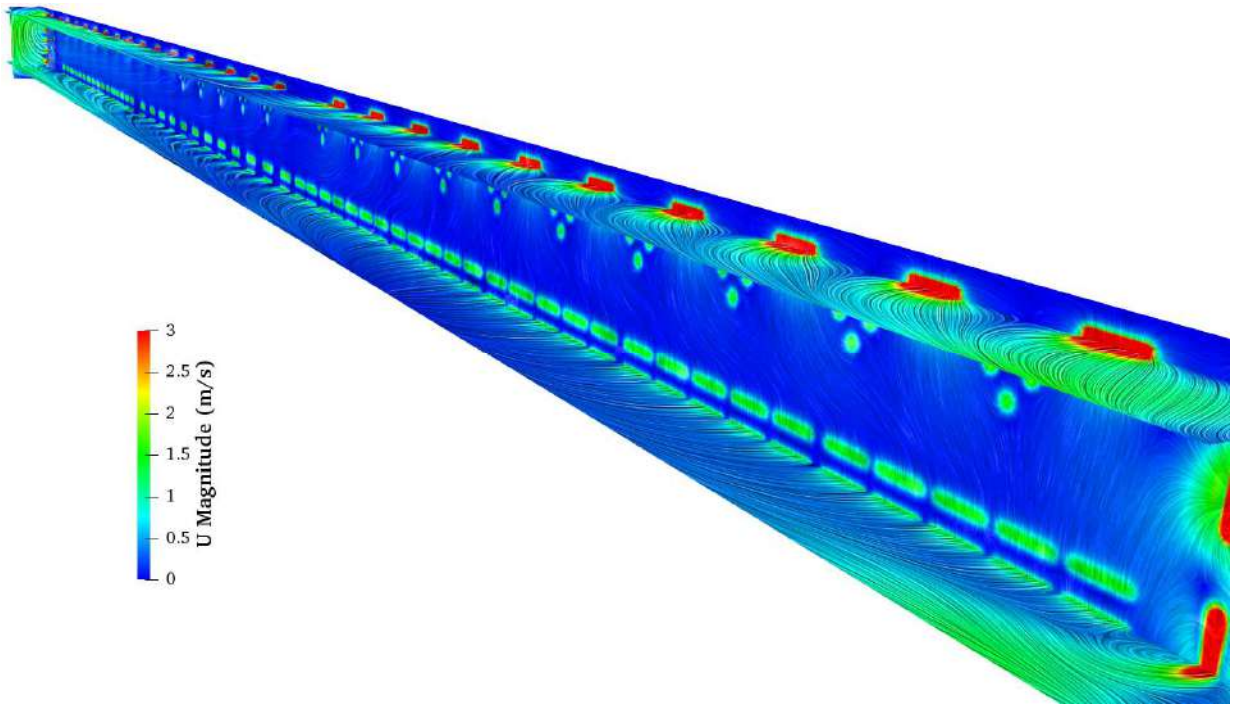

FIGURE 14: THE STREAMLINE VISUALIZATION ALONG WITH THE CURING OVEN CRITICAL PLANES ($t = 3\,Min$), USING THE LIC (LINE INTEGRAL CONVOLUTION) APPROACH [25].

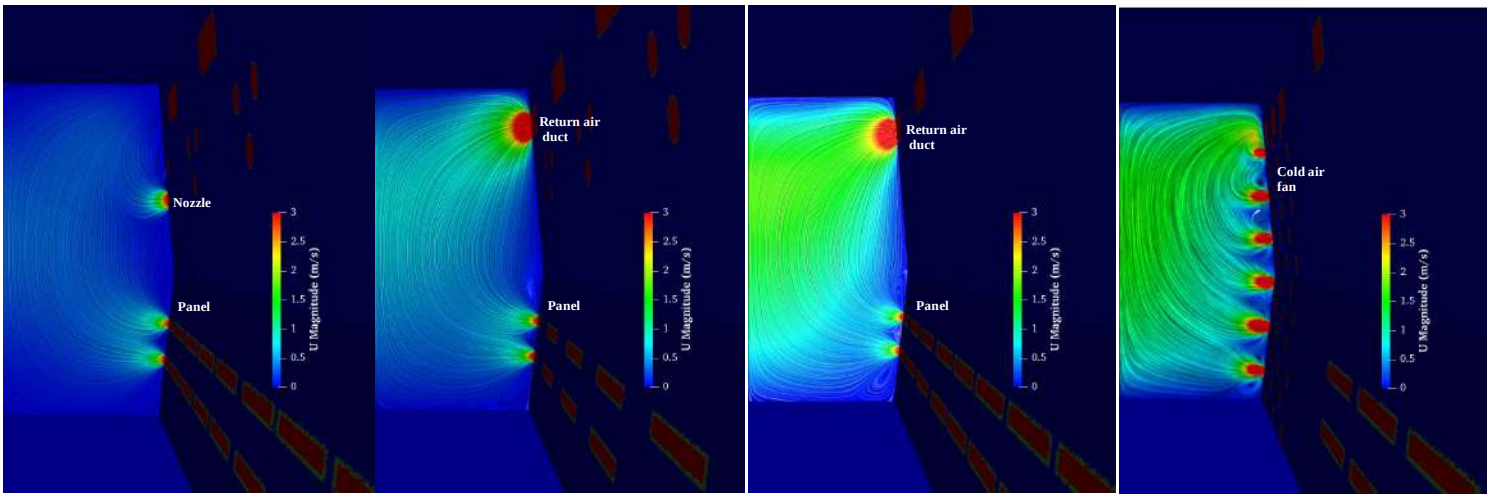

(a) *Zone*2 ($L_1 = 10\,m$) (b) *Zone*3 ($L_2 = 24\,m$) (c) *Zone*4 ($L_3 = 39\,m$) (d) *Zone*6 ($L_4 = 49\,m$)

FIGURE 15: THE CONTOUR OF VELOCITY MAGNITUDE WITH VORTICAL STRUCTURES (LIC VISUALIZATION) AT VARIOUS LOCATIONS OF THE AUTOMOTIVE CURING OVEN ($t = 3\,Min$).

6. CONCLUSION

The current simulation used the OpenFOAM framework as a reliable tool and open-source software to simulate the conduction and convection processes in the oven's conjugate heat transfer mechanism. An accurate LES turbulence model and a reasonably fine grid spacing next to components yield a precise result. *The accuracy of the conjugate heat transfer code is validated by heat sink case examination and good agreements with experimental values observed.* Quantitative velocity and temperature convective fields, as well as flow streamline detection, are explained in detail for all length of the oven. *According to simulation results, the applied low-cost optimization, manipulating the intake hot flow rate, achieved significant energy efficiency improvement during the oven's length.*

ACKNOWLEDGEMENTS

This work was supported by Project "MOSIPO", project grant no. POCI-01-0247-FEDER-072621. The research was also partly supported by CMAST Center for Mechanical and Aerospace Science and Technology, research unit No. 151 (Project UID/00151/2020) from Fundacao para a Ciencia e Tecnologia (Portugal).

REFERENCES

[1] Ajah, V. and Ejiogu, E., 2019. Solar Thermal/Electricity Paint Curing Oven. In 2019 IEEE International Conference on Sustainable Energy Technologies and Systems (ICSETS) (pp. 075-080). IEEE.

[2] Ashrafizadeh, A., Mehdipour, R. and Rezvani, M., 2009, October. An efficient and accurate numerical simulation method for the paint curing process in auto industries. In ICADME Conference, Malaysia.

[3] Cavalcante, E.S., Vasconcelos, L.G.S., de Farias Neto, G.W., Ramos, W.B. and Brito, R.P., 2020. Automotive painting process: Minimizing energy consumption by using adjusted convective heat transfer coefficients. Progress in Organic Coatings, 140, p.105479.

[4] Streitberger, H.J. and Dossel, K.F. eds., 2008. Automotive paints and coatings. John Wiley & Sons.

[5] Niamsuwan, S., Kittisupakorn, P. and Suwatthikul, A., 2015. Enhancement of energy efficiency in a paint curing oven via CFD approach: Case study in an air-conditioning plant. Applied Energy, 156, pp.465-477.

[6] Rao, P. and Teeparthi, S., 2011, January. A semi–computational method to predict body temperatures in an automotive paint bake oven. In ASME International Mechanical Engineering Congress and Exposition (Vol. 54891, pp. 85-95).

[7] Wu, Y.H., Srinivasan, K., Patterson, S. and Bot, E., 2013, July. Transient thermal analysis for the automotive underhood and underbody components. In Heat Transfer Summer Conference (Vol. 55508, p. V004T14A028). American Society of Mechanical Engineers.

[8] Mulemane, A., Hurst, L., Fraser, A. and Sinclair, J., 2015. A reduced order model for simulating heat transfer processes in automotive paint shop ovens (No. 2015-01-0030). SAE Technical Paper.

[9] Despotovic, M. and Babic, M., 2018. Analysis of different scenarios of car paint oven redesign to achieve desired indoor air temperature. Energy Efficiency, 11(4), pp.877-891.p

[10] Nazif, H.R., 2019. Improving the thermal efficiency of a car wax oven using CFD simulation and measurement. International Journal of Modelling and Simulation, 39(2), pp.125-134.

[11] Xiao, J., Li, J., Lou, H.H. and Huang, Y., 2006. Cure-window-based proactive quality control in topcoat curing. Industrial & engineering chemistry research, 45(7), pp.2351-2360.

[12] Giampieri, A., Ling-Chin, J., Ma, Z., Smallbone, A. and Roskilly, A.P., 2020. A review of the current automotive manufacturing practice from an energy perspective. Applied Energy, 261, p.114074.

[13] Pendar, M.R. and Páscoa, J.C., 2021. Numerical analysis of charged droplets size distribution in the electrostatic coating process: Effect of different operational conditions. Physics of Fluids, 33(3), p.033317.

[14] Pendar, M.R. and Roohi, E., 2015, November. Detailed investigation of cavitation and supercavitation around different geometries using various turbulence and mass transfer models. In Journal of Physics: Conference Series (Vol. 656, No. 1, p. 012070). IOP Publishing.

[15] Pendar, M.R. and Pascoa, J., 2021. Study of the Plasma Actuator Effect on the Flow Characteristics of an Airfoil: An LES Investigation. SAE

International Journal of Advances and Current Practices in Mobility, 3(2021-01-0016), pp.1206-1215.

[16] Pendar, M.R. and Pascoa, J., 2021. Numerical Simulation of the Electrostatic Coating Process: the Effect of Applied Voltage, Droplet Charge and Size on the Coating Efficiency. SAE International Journal of Advances and Current Practices in Mobility, 3(2021-01-0022), pp.1223-1230.

[17] Energy, U.S.D.o., Technology roadmap for energy reduction in automotive manufacturing; 2008.

[18] Seog-Chan, Hildreth OH. Analytics for smart energy management: tools and applications for sustainable manufacturing. Springer; 2018.

[19] Pendar, M.R. and Roohi, E., 2018. Cavitation characteristics around a sphere: An LES investigation. International Journal of Multiphase Flow, 98, pp.1-23.

[20] Pendar, M.R. and Páscoa, J.C., 2022. Numerical Investigation of Plasma Actuator Effects on Flow Control Over a Three-Dimensional Airfoil With a Sinusoidal Leading Edge. Journal of Fluids Engineering, 144(8), p.081208.

[21] Pendar, M.R. and Páscoa, J.C., 2020. Atomization and spray characteristics around an ERBS using various operational models and conditions: numerical investigation. International Journal of Heat and Mass Transfer, 161, p.120243.

[22] da Silva, V.A., de Neves Gomes, L.A.C., de Lima e Silva, A.L.F. and de Lima e Silva, S.M.M., 2019. Analysis of natural convection in heat sink using OpenFOAM and experimental tests. Heat and Mass Transfer, 55(8), pp.2289-2304.

[23] Harahap, F. and Rudianto, E., 2005. Measurements of steady-state heat dissipation from miniaturized horizontally-based straight rectangular fin arrays. Heat and mass transfer, 41(3), pp.280-288.

[24] Magnusson, J., 2010. Conjugate HeatFoam with explanational tutorial together with a buoyancy driven flow tutorial and a convective conductive tutorial. Magnusson's Technology Center, Chalmers University of Technology, Gothenburg.

[25] Stalling, D. and Hege, H.-C., 1997. LIC on Surfaces. Texture Synthesis with Line Integral Convolution, pp. 51-64.